Turkish Journal of Earth Sciences

http://journals.tubitak.gov.tr/earth/

Research Article

Turkish J Earth Sci
(2020) 29: 242-256

doi:10.3906/yer-1812-13

Upper Paleocene-lower Eocene calcareous nannofossil stratigraphy at the Misheiti Section, Central Sinai, Egypt

Atef M. KASEM[1,*], Sherwood WISE Jr.[2], Mahmoud M. FARIS[3], Sherif FAROUK[4], Esam ZAHRAN[1]

[1]Department of Geology, Faculty of Science, Damanhour University, Damanhour, Egypt
[2]Department of Earth, Ocean, and Atmospheric Science, College of Arts and Sciences, Florida State University, Tallahassee, FL, USA
[3]Department of Geology, Faculty of Science, Tanta University, Tanta, Egypt
[4]Egyptian Petroleum Research Institute, Nasr City, Egypt

Received: 21.12.2018 • **Accepted/Published Online:** 05.09.2019 • **Final Version:** 15.01.2020

Abstract: Calcareous nannofossil, $\delta^{13}C$, $\delta^{18}O$, and carbonate content data were used to define and reveal the variations across the latest Paleocene-earliest Eocene interval at the Misheiti Section, Central Sinai, Egypt. The upper part of Tarawan Formation, the Esna Formation, and the lowermost Thebes Formation were included in this study. In this study, the Esna Formation is informally divided into Hanadi/Mahmiya and Abu Had members. Four calcareous nannofossil zones (NP9, NP10, NP11, and NP12) and four subzones (NP9a, NP9b, NP10a, and NP10b) were recognized. The biostratigraphic importance of significant calcareous nannofossil bioevents associated with the P/E boundary was discussed. The LOs of *Rhomboaster* spp., *Discoaster araneus*, and/or *D. anartios* were used to delineate the base of earliest Eocene Subzone NP9b within the lower part of the Esna Formation. The global decreases of $\delta^{13}C$, $\delta^{18}O$, and carbonate contents at the P/E boundary were documented in the study section.

Key words: Nannofossils, carbon and oxygen isotopes, carbonate content, Paleocene-Eocene boundary, *Rhomboaster*

1. Introduction

Significant micropaleontological, sedimentological, and isotopic changes mark the Paleocene/Eocene (P/E) boundary (Dupuis et al., 2003). It was associated with a short time of global warming (Westerhold et al., 2009), a global drop in δ^{13} C (Sluijs et al., 2006), and a global increase in kaolinite indicating an interval of high humidity (Robert and Kennett, 1992), as well as faunal and floral turnovers, originations, and migration towards higher latitudes (Dupuis et al., 2003). The cause(s) and scenarios of these changes are a point of arguments (Bains et al., 1999).

During the Paleocene-Eocene transition, Egypt was situated at the southern margin of the Tethys Sea. It is considered a key region for studying chemical and biologic variations at the P/E boundary, where the sedimentation rates were high (Tantawy, 2006). The GSSP for the base of the Eocene has been formally placed at Dababiya in Egypt (Dupuis et al., 2003). The best characteristic for delineating the base of the Eocene at the GSSP section is the onset of the global Carbon Isotope Excursion that is coincident with the major Benthonic Foraminifera Extinction Event (BFE; Thomas et al., 2000; Dupuis et al., 2003). It is also coincident with distinct marker beds known as the Dababiya Quarry Beds (DQBs; Dupuis et al., 2003) that were documented in several sections in Egypt (Tantawy, 2006; Khozyem et al., 2013).

2. Studied section and methods

Twenty-two bulk rock samples were investigated from the upper Paleocene-lower Eocene at the Misheiti Section, Central Sinai, Egypt (Figure 1). Smear slides were prepared according to Bown and Young (1998) and investigated using a Zeiss Axio-Photo microscope at Florida State University, USA. We counted 300–400 calcareous nannofossil specimens on the slide to recognize the relative abundances of species (Jiang and Gartner, 1986). The calcareous nannofossil diversity represents the total number of species recorded in the sample. *Thoracosphaera* fragments greater than 4 μm were counted as a whole specimen (Gardin and Monechi, 1998). The state of preservation of the assemblage was described as good (G) for little or no evidence of etching and/or overgrowth, and moderate (M) when specimens exhibited some overgrowth and/or dissolution but the species was still recognizable (Kasem et al., 2017a). The calcium carbonate

* Correspondence: kasematef@yahoo.com

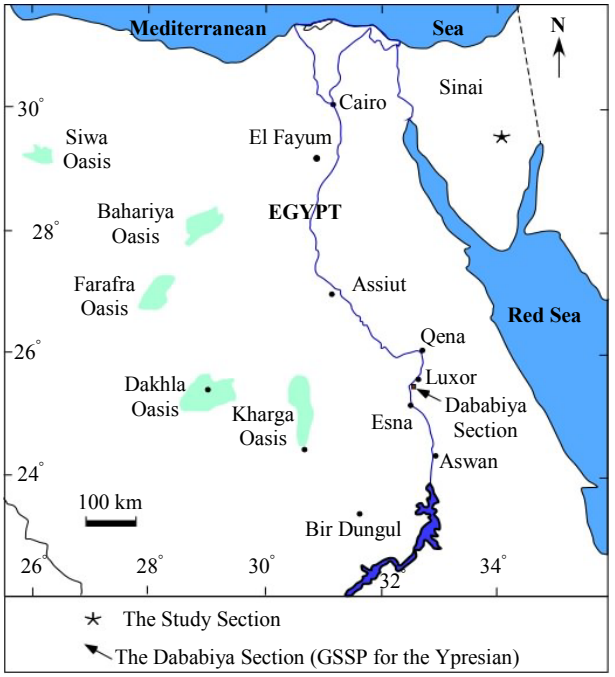

Figure 1. Location map. The star indicates the location of the study section and the arrow indicates the Dababiya GSSP section for the base of the Eocene.

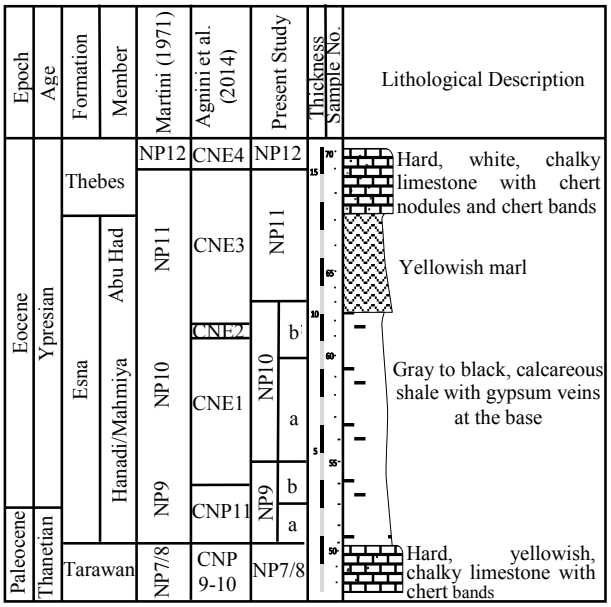

Figure 2. A lithological log of the upper Paleocene-lower Eocene at Misheiti.

content and $\delta^{13}C$ and $\delta^{18}O$ analyses were carried out using a Thermo Fischer Scientific Delta Plus XP isotope ratio mass spectrometer at the National High Magnetic Field Laboratory, Florida State University, USA.

3. Lithostratigraphy

The uppermost Paleocene-lower Eocene at the Misheiti Section is divided into three rock units (Figure 2), as follows.

3.1. The Tarawan Formation

Tarawan Formation was introduced to describe a bed of chalk grades into chalky limestones and marly limestone at the Gebel Tarawan section, Kharga Oasis, Western Desert, Egypt (Awad and Ghobrial, 1965). In this study, the covered part of the Tarawan Formation consists of hard, yellowish chalky limestone conformably overlain by the Esna Formation (Figure 2).

3.2. The Esna Formation

Beadnell (1905) introduced the Esna Shale to describe 104-m-thick greenish-gray shale with calcareous interbeds passing upward into light-gray argillaceous limestone that overlies the Cretaceous succession and underlies the Eocene sequence at Gabal Oweina, near Esna, Nile Valley, Egypt. Later, Said (1960) assigned this unit to the Esna Formation. This unit was dated as Thanetian-Ypresian. The Esna Formation at the study section is about 11.7 m of gray calcareous shale and grades upward to yellowish marl (Figure 2).

The Esna Formation was subdivided into different units by various authors (Abdel Razik, 1972; Dupuis et al., 2003; Tantawy, 2006). In our study, the Esna Formation was informally subdivided into the Hanadi/Mahmiya and Abu Had members (Figure 2).

3.2.1. The Hanadi/Mahmiya Member

The Hanadi Member was established by Abdel Razik (1972) to cover from the base of the Esna Formation to the top of the phosphatic bed (Aubry et al., 2007). Aubry et al. (2007) restricted this member to the lower part of the Esna Formation below the Dababiya Quarry Member. Aubry et al. (2007) also introduced the Mahmiya Member to describe monotonous, dark shales with less than 50% calcium carbonate content at the Dababiya Section. In our present study, the lower 8.2 m of dark gray calcareous shale in the Esna Formation are informally assigned to the Hanadi/Mahmiya Member (Figure 2).

3.2.2. The Abu Had Member

This member was suggested by Abdel Razik (1972) to describe interbeds of limestones and shales in the lowermost Thebes Formation. Aubry et al. (2007) assigned this member to the Esna Formation. In the study section, this member is 3.5-m-thick yellowish marl (Figure 2).

3.3. The Thebes Formation

The Thebes Formation was originally assigned by Said (1960) to describe a 290-m white to grayish white limestone with many flint bands above the Esna Formation at Gabal

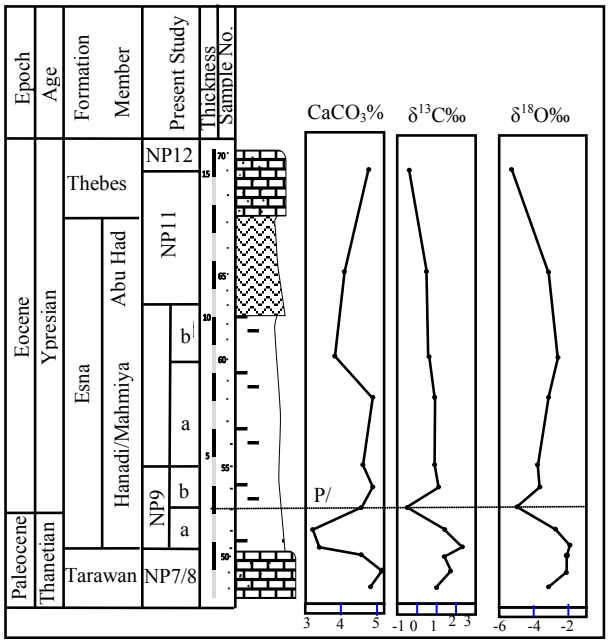

Figure 3. Variations of carbonate content, $\delta^{13}C$, and $\delta^{18}O$ across the P/E transition at the Misheiti Section, Central Sinai, Egypt.

Gurnah, Nile Valley, Egypt. This formation was assigned to the Ypresian. About 2.5 m of hard white, chalky limestone with chert bands and nodules in the lower part of the Thebes Formation are included in this study (Figures 2 and 3).

4. Biostratigraphy

Martini's (1971) zonation scheme complemented by Aubry et al. (1999) was followed in our study. In addition, significant calcareous nannofossil bioevents and their biostratigraphic significance are discussed. Abbreviations utilized in the present study include LO (lowest occurrence), where the first specimen was recognized, and HO (highest occurrence), for the last appearance of the taxon in the section. The Table shows the stratigraphic distributions of calcareous nannofossil taxa. Microphotographs of most taxa are shown in Figures 4 and 5. Five calcareous nannofossil zones and four subzones are recognized and discussed below.

4.1. *Discoaster mohleri* Zone (NP7/8) (Hay, 1964; emended by Romein, 1979)

The *Discoaster mohleri* Zone covers the sequence from the LO of *Discoaster mohleri* to the LO of *D. multiradiatus* and is assigned to the Thanetian (Kasem et al., 2017b). This zone occurs within the Tarawan Formation (Figure 2). The *Discoaster mohleri* Zone is comparative to Martini's (1971) Zones NP7 and NP8, Okada and Bukry's (1980) Zones CP6 and CP7, and Zones CNP9 and CNP10 of Agnini et al. (2014). It is hard to record *Heliolithus riedelii* in many sections (Perch-Nielsen, 1985) and several studies documented disagreements in its range at different locations (Romein, 1979; Agnini et al., 2007a). As such, *Heliolithus riedelii* is biostratigraphically unreliable (Agnini et al., 2007a). Bukry (1973) used *Discoaster nobilis* in place of *H. riedelii*, but the LOs of *D. nobilis* and *D. multiradiatus* were found coincident (e.g., Romein, 1979). Therefore, Romein (1979) suggested the combination of the *D. mohleri* and *H. riedelii* Zones into the *D. mohleri* Zone (NP7/8), and this combination is adopted here.

4.2. *Discoaster multiradiatus* Zone (NP9) (Bramlette and Sullivan, 1961; emended by Martini, 1971)

This zone covers the sequence from the LO of *Discoaster multiradiatus* to the LO of *Tribrachiatus bramlettei*. It is assigned a Thanetian-Ypresian age and is about 3 m in the Esna Formation (Figure 2). The *Discoaster multiradiatus* Zone is comparable to Zone NP9 (Martini, 1971), Zone CN8 (Okada and Bukry, 1980), and Subzone NTp16b to Zone NTp20 (Varol, 1989). In Egypt, the *D. multiradiatus* Zone (NP9) was recorded in several localities (see Aubry and Salem, 2013b, and references therein; Al Wosabi, 2015; Faris et al., 2015).

Further subdivisions of Zone NP9 were suggested by various authors. Bukry (1973) subdivided Zone CP8 (=Zone NP9 of Martini, 1971) into two subzones. He stated that the upper part of the zone (the *Campylosphaera eodela* Subzone) can be delineated by the first appearance of *Campylosphaera eodela*, in deep-ocean areas, and by *C. eodela*, *Rhomboaster cuspis*, and related taxa in shallow-ocean areas (Bukry and Percival, 1971). This agrees well with the occurrences reported by several authors (e.g., Perch-Nielsen, 1985; Tantawy, 2006). However, Agnini et al. (2007a) observed that *Campylosphaera* occurs in the Paleocene interval of Zone NP9, and they noted various stratigraphic ranges for this taxon. In this study, *C. dela*, which is lumped with *C. eodela* (see below), is recorded within Zone NP7/8 (Table).

Further subdivision of Zone NP9 into Subzones NP9a and NP9b were carried out by Bybell and Self-Trail (1997) on the basis of the disappearance of *Fasciculithus* species (e.g., *F. clinatus*, *F. hayi*, *F. lillianae*, *F. alanii*, *F. bobii*, and *F. mitreus*). However, Khozyem et al. (2013) documented the disappearance of these species in the middle of Zone NP9 and suggested that this change is possibly a result of carbonate dissolution. Furthermore, *F. involutus* plus *F. tympaniformis* occur in the basal part of Zone NP10 in the present study (Table). Similarly, Aubry et al. (1999) subdivided Zone NP into two subzones depending on the LOs of *Rhomboaster* spp., and/or *D. araneus*. This subdivision suggestion was followed by many authors (e.g., Dupuis et al., 2003; Raffi et al., 2005; Agnini et al., 2007a, 2007b; Faris and Abu Shama, 2007; Faris et al.,

Table. Distribution chart of calcareous nannofossil taxa across the P/E transition at the Misheiti Section, Central Sinai, Egypt (continued).

Paleocene			Eocene																						Epoch
Thanetian			Ypresian																						Age
Tarawan			Esna														Thebes								Formation
			Hanadi/Mahmiya													Abu Had									Member
NP7/8			NP9				NP10									NP11							NP12		Nannofossil Zone
			a		b		a							b											
M	M	M	C	C	G	M	G	G	G	M	G	G	M	G	G	G	G	G	G	G	G	G	G	G	Preservation
C	A	C	C	C	A	C	A	A	A	F	A	C	C	A	C	C	C	C	C	C	C	C	C	C	Abundance
48	49	50	51	52	53	54	55	56	57	58	59	60	61	62	63	64	65	66	67	68	69	70	Sample number		
F	R	R	C																				*Bomolithus elegans*		
R	F	F	R		R	C	F	A	C	C	C	C	C	R	R	F	R	F			R	R	*Campylosphaera dela*		
C	C	C	C	C	C	A	C	A	C	A	C	A	A	C	F	C	R	C	C	C	C	F	*Coccolithus pelagicus*		
R	C	C		R																			*Cruciplacolithus tenuis*		
C	R	R	R	F			R		R														*Discoaster mohleri*		
F	R	R				R	C		C	C	C	F	F	C	R	F		R					*Ellipsolithus macellus*		
R	F	F		F	F	F	F		C			C		C		R			R				*Ericsonia robusta*		
C	A	A	C	A	A	A	A	A	A	A	A	A	A	A	C	C	C	C	C	A	A	A	*Ericsonia subpertusa*		
A	A	A	C	A		C	C	C	C	C	C	C											*Fasciculithus tympaniformis*		
F	F	F			R		R											R					*Neochiastozygus modestus*		
F	C	C				F	F	F	F		R	C	F										*Prinsius martinii*		
F	R	R			R		F	F	R	R	F	R		C	F	C	F	R	R	R	R		*Thoracosphaera operculata*		
R	R	R		R					R														*Toweius eminens*		
F	F	F				C	C	R	F				R							R			*Toweius pertusus*		
F	C	C		F		C	F	F				R		F									*Toweius tovae*		
C	R	R	A	C	C	A	C	A	A	A	A	A	A	A	C	A	A	C	F	C	A	C	*Sphenolithus primus*		
	F	F				C	C	C	C	F	C	F		R				R			R		*Chiasmolithus consuetus*		
	R	R				C	C	C	C	C	F	R	R	R	R	R	R	R					*Neochiastozygus junctus*		
	F	F					R	F															*Sphenolithus anarrhopus*		
	F						F											R					*Zeugrhabdotus sigmoides*		
			A	R																			*Bomolithus megastypus*		
			R			F				R													*Discoaster falcatus*		
			C			F																	*Discoaster lenticularis*		
			C	C	C	C	C	C	F	R	F	C	C											*Discoaster multiradiatus*		
			R																				*Lithoptychius billii*		
			R	F	R																		*Fasciculithus alanii*		
			R	R	R																		*Fasciculithus inversus*		
			R	C	C																		*Fasciculithus thomasii*		
			R	R	C	R	R																*Lithoptychius sp.*		
			C																				*Lithoptychius stegastos*		
				R					R														*Discoaster nobilis*		
				R	R																		*Ellipsolithus distichus*		
				F		F																	*Fasciculithus lillianiae*		
				R																			*Fasciculithus* **aff.** *lillianiae*		
				R																			*Fasciculithus mitreus*		
				R																			*Fasciculithus richardi*		
				R	R	F	F																*Fasciculithus involutus*		
				R			F																*Heliolithus kleinpellii*		

Table. (Continued).

Paleocene			Eocene																						Epoch
Thanetian			Ypresian																						Age
Tarawan			Esna																Thebes						Formation
			Hanadi/Mahmiya														Abu Had								Member
NP7/8			NP9				NP10										NP11						NP12		Nannofossil Zone
			a		b		a						b												
MC	MA	MC	MC	MC	GA	MC	GA	GA	GA	MF	GA	MC	GA	GC	GC	GC	GC	GC	GC	GC	GC	GC	GC	GC	Preservation
C	A	C	C	C	A	C	A	A	A	F	A	C	A	C	C	C	C	C	C	C	C	C	C	C	Abundance
48	49	50	51	52	53	54	55	56	57	58	59	60	61	62	63	64	65	66	67	68	69	70	Sample number		
					C																				*Discoaster anartios*
					R	C	R	R		R	R	R	F		R	R	R	R							*Discoaster araneus*
					R					R	R		R		R	R									*Discoaster paelikei*
					C	F	F			R																*Rhomboaster bitrifida*
					C	C		R	C	F	C	C														*Rhomboaster cuspis*
					R																				*Rhomboaster intermedia*
					R	R																			*Tribrachiatus spineus*
						F	R			R	R	F	F	R						R					*Chiasmolithus bidens*
						R																			*Discoaster mahmoudi*
						R	R			R															*Neochiastozygus perfectus*
						F	R	C	C		R	R	C	R	R			C	C	C	C				*Toweius callosus*
							C	A	C			R	R	C		R	R			R	R				*Blackites herculesii*
	4						R																		*Chiasmolithus edentulus*
							R	R				R						R							*Neochiastozygus distentus*
							R	R	R	F	F	C	R												*Tribrachiatus bramlettei*
								R			R					R		R		F	C	R			*Biantholithus sparsus*
								F	R	F	R	C	F	R	F	R	R	R		R	R				*Discoaster binodosus*
								R		F		R	R	R	R	R	R								*Discoaster diastypus*
										R															*Tribrachiatus digitalis*
										R															*Scyphosphaera* **spp.**
											C														*Coccolithus crucis*
												C	R	R											*Tribrachiatus contortus*
												R					R		R	R	C				*Cyclicargolithus luminis*
												R													*Chiasmolithus solitus*
												R	F		F	F	F	C	F	C	C	C			*Sphenolithus radians*
													F	C	F						F				*Sphenolithus editus*
													F	C	R	C	F			R	R				*Sphenolithus villae*
													R		R	R	R			R	R				*Chiasmolithus grandis*
													R	R	R	C	R	R		R	R	R			*Zygrhablithus bijugatus*
														R	R	R	R				R				*Discoaster barbadiensis*
														R	R						R				*Pontosphaera exilis*
														C	F	C	C	R	R	R					*Tribrachiatus orthostylus*
															R	R		R	R	R	R	R			*Pontosphaera pectinata*
																R									*Markalius inversus*
																					R	R			*Discoaster lodoensis*
																					R	R			*Zygodiscus plectopons*

Abundance
VA: Very Abundant (>10 specimens/field of view)
A: Abundant (1-10 specimens/field of view)
C: Common (1 specimen/1-10 fields of view)
F: Few (1 specimen/1-50 fields of view)
R: Rare (1 secimen/>50 fields of view)
Preservation
G: Good, M: Moderate, P: Poor

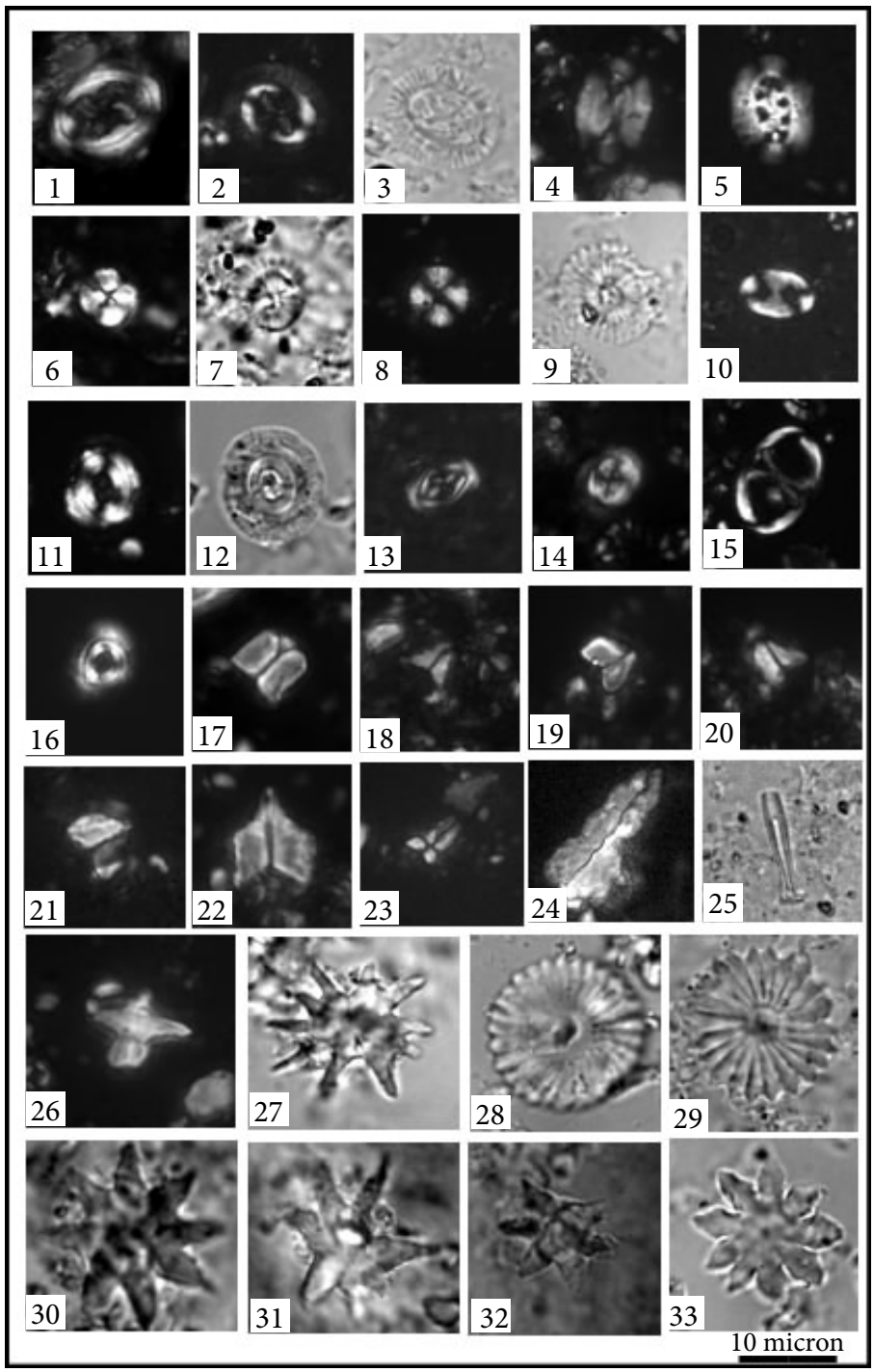

Figure 4. 1- *Chiasmolithus grandis*. Sample No. 61, Subzone NP10b. 2, 3- *Chiasmolithus consuetus*. Sample No. 54, Subzone NP9b. 4- *Ellipsolithus macellus*. Sample No. 54, Subzone NP9b. 5- *Ellipsolithus distichus*. Sample No. 52, Subzone NP9a. 6–9- *Bomolithus megastypus*. Sample No. 51, Subzone NP9a. 10- *Pontosphaera exilis*. Sample No. 69, Zone NP12. 11, 12- *Ericsonia subpertusa*. Sample No. 61, Subzone NP10b. 13- *Campylosphaera dela*. Sample No. 56, Subzone NP10a. 14- *Toweius pertusus*. Sample No. 56, Subzone NP10a. 15- *Neochiastozygus junctus*. Sample No. 61, Subzone NP10b. 16- *Toweius callosus*. Sample No. 54, Subzone NP9b. 17- *Fasciculithus involutus*. Sample No. 52, Subzone NP9a. 18- *Fasciculithus thomasii*. Sample No. 52, Subzone NP9a. 19, 20- *Fasciculithus alanii*. 19, Sample No. 51, Subzone NP9a; 20, Sample No. 52, Subzone NP9a. 21, 22- *Fasciculithus lillianiae*. Sample No. 52, Subzone NP9a. 23- *Sphenolithus radians*. Sample No. 60, Subzone NP10b. 24- *Zygrhablithus bijugatus*. Sample No. 64, Zone NP11. 25- *Blackites herculesii*. Sample No. 64, Zone NP11. 26- *Discoaster diastypus*. Sample No. 56, Subzone NP10a. 27- *Discoaster anartios*. Sample No. 53, Subzone NP9b. 28, 29- *Discoaster multiradiatus*. 28, Sample No. 54, Subzone NP9b; 29, Sample No. 65, Zone NP11. 30–32- *Discoaster araneus*. 30, 32- Sample No. 61, Subzone NP10b; 31- Sample No. 66, Zone NP11. 33- *Discoaster binodosus*. Sample No. 58, Subzone NP10a.

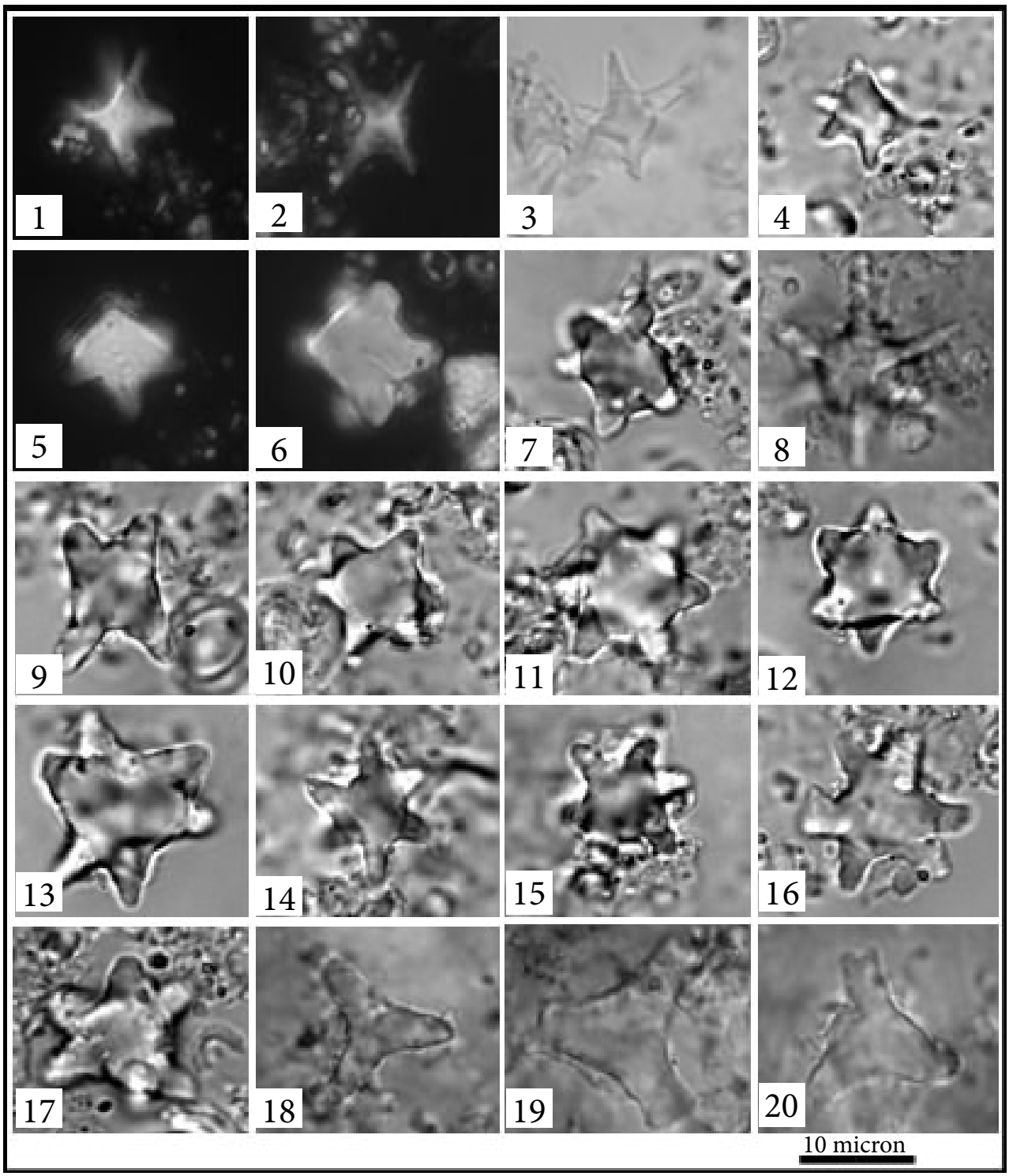

Figure 5. 1, 2- *Rhomboaster calcitrapa*. 1, Sample No. 54, Subzone NP9b; 2, Sample No. 53, Subzone NP9b. 3, 4- *Rhomboaster bitrifida*. 3, Sample No. 53, Subzone NP9b; 4, Sample No. 58, Subzone NP10a. 5–7- *Rhomboaster cuspis*. Sample No. 58, Subzone NP10a. 8- *Tribrachiatus spineus*. Sample No. 53, Subzone NP9b. 9–12- *Tribrachiatus bramlettei*. 9, Sample No. 60, Subzone NP 10b; 10–12- Sample No. 58, Subzone NP10a. 13–17- *Tribrachiatus contortus*. 13, 15, 16, Sample No. 60, Subzone NP10b; 14, Sample No. 58, Subzone NP10a, 17, Sample No. 62, Subzone NP10c. 18–20- *Tribrachiatus orthostylus*. 18, Sample No. 67, Zone NP11; 19, 20, Sample No. 65, Zone NP11.

2015). In our present study, Zone NP9 is subdivided into two subzones (Table; Figure 2).

4.2.1. Subzone NP9a

Aubry et al. (1999) introduced Subzone NP9a to span from the LO of *Discoaster multiradiatus* to the LOs of *Rhomboaster* spp., *D. araneus*, and/or *D. anartios*. This subzone is about 1.5 m in the Esna Formation (Figure 2) and is assigned a Thanetian age. Previous studies showed that the LOs and HOs of *Rhomboaster* spp., *Discoaster araneus*, and *D. anartios* are restricted to the Paleocene-Eocene interval (Dupuis et al., 2003; Tantawy, 2006; Agnini et al., 2007a, 2007b; Aubry et al., 2007; Faris and Salem, 2007; Aubry and Salem, 2013a). The *Rhomboaster-Discoaster* Calcareous Nannofossil Excursion Taxa (CNET, Bown and Pearson, 2009) were considered as the most significant bioevent across the P/E boundary (Dupuis et al., 2003). However, the Eocene sequence at the Dababiya Section starts at the base of an interval (~73 cm) characterized by carbonate dissolution overlain by sediments that contain *D. araneus*, *D. anartios*, and *Rhomboaster* spp. (Dupuis et al., 2003). Therefore, the exact range of nannofossil species across the P/E interval is inadequately known. Faris and Salem (2007) used the HO of *Fasciculithus alanii* plus the LOs of *R. intermedia*, *R. calcitrapa*, and *Rhabdosphaera solus* (*Blackites herculesii* herein; Table) to delineate the base of Subzone NP9b.

4.2.2. Subzone NP9b

Aubry et al. (1999) introduced Subzone NP9b to span the interval between the LO of *Rhomboaster* spp., *Discoaster araneus*, and/or *D. anartios* to the LO of *Tribrachiatus bramlettei.* It is assigned to the Ypresian. This subzone is 1.5 m in the Esna Formation at the Misheiti Section (Figure 2). Agnini et al. (2014) included all *Fasciculithus* species that first appear in Zone NP9 in a single group, the *F. richardii* group. They used the HOs of the *F. richardii* group and *F. tympaniformis* to place the lower and upper limits of Zone CNE1, respectively.

Abu Shama et al. (2007) noted that the HO of *Fasciculithus alanii* is coincident with the base of Subzone NP9b. However, it disappears in the uppermost of Subzone NP9a at the Dababiya area (Dupuis et al., 2003). In the present study, most fasciculith species disappear within Subzone NP9a (Table). However, *F. involutus*, *F. tympaniformis*, and *F. thomasii* cross the NP9a/NP9b subzonal boundary (Table).

4.3. *Tribrachiatus contortus* Zone (NP10) (Hay, 1964)

This zone was introduced to span the interval from the LO of *Tribrachiatus bramlettei* to the HO of *T. contortus*. It is assigned to the Ypresian and is about 5.6 m within the Esna Formation at the Misheiti Section (Figure 2). This zone is correlative to Martini's (1971) Zone NP10 and Okada and Bukry's (1980) Subzone CP9a. The HO of fasciculiths often occurs in the basal part of Zone NP10 (Romein, 1979). Therefore, it can approximately trace the entry of Zone NP10 when *Tribrachiatus* is rare or absent (Perch-Nielsen, 1985; Tantawy, 2006; Faris and Abu Shama, 2007). However, *F. tympaniformis* extends with common abundance to the middle portion of Zone NP10 in the study section (Table). Abu Shama et al. (2007) used the increased frequency of *Neochiastozygus junctus* to delineate the lower limit of Zone NP10. In the present study, *N. junctus* increases remarkably just below the NP9/NP10 zonal boundary (Table).

Aubry (1996) utilized the total ranges of *Tribrachiatus digitalis* and *T. contortus* to further subdivide Zone NP10 into four subzones. Several studies confirmed the validity of this subdivision (e.g., Bybell and Self-Trail, 1997; Dupuis et al., 2003; Tantawy, 2006; Abu Shama et al., 2007; Faris and Salem, 2007; Al Wosabi, 2015). The subdivision of Aubry (1996) ensures the completeness of Zone NP10, but the systematic position and the range of *T. digitalis* were criticized (e.g., Wei and Zhong, 1996; Raffi et al., 2005).

The evolution within the *Tribrachiatus* lineage is characterized by subsequent flattening and rotation, as well as the merging of the two "triplets" (e.g., Wei and Zhong, 1996). Aubry (1996) differentiated between *T. digitalis* marked by well-merged "triplets", *T. contortus* marked by well-differentiated "triplets", and *T. orthostylus* characterized by indistinct "triplets". On the other hand, Wei and Zhong (1996) considered *T. digitalis* as a variant of *T. contortus*. In the original description and later studies, *T. digitalis* first occurs below the LO of *T. contortus* (e.g., Aubry, 1996; Dupuis et al., 2003; Tantawy, 2006). However, it was recorded in association with *T. contortus* (Raffi et al., 2005; Agnini et al., 2007a). Furthermore, *Tribrachiatus* specimens resembling *T. digitalis* were recorded with *T. contortus* and were considered transitional forms between *T. contortus* and *T. orthostylus* (Raffi et al., 2005; Agnini et al., 2007a). Raffi et al. (2005) reported that the intermediate form between *T. contortus* Type B and *T. orthostylus* Type A is Aubry's (1996) *T. digitalis* morphotype. Moreover, *T. digitalis* has a short range and is often rare (Aubry, 1996; Dupuis et al., 2003; Tantawy, 2006). In addition, inconsistent durations of the total range of *T. digitalis* were documented (Berggren and Aubry, 1996). Nevertheless, Subzones NP10a and NP10c of Aubry (1996) cannot be differentiated when *T. digitalis* is absent. Therefore, we prefer to avoid using *T. digitalis* as a marker and recommend subdividing Zone NP10 based on the LO of *T. contortus* into Subzones NP10a and NP10b.

4.3.1. Subzone NP10a

Aubry (1996) introduced Subzone NP10a to range from the LO of *Tribrachiatus bramlettei* to the LO of *T. contortus.* This subzone is about 3.9 m thick in the Esna Formation (Table; Figure 2), and is assigned to the Ypresian. This

subzone is equivalent to Aubry's (1996) Subzones NP10a, NP10b, and NP10c and Tantawy's (1998) Subzones NP10a and NP10b.

4.3.2. Subzone NP10b

Aubry (1996) originally introduced Subzone NP10b to span the total stratigraphic range of *Tribrachiatus contortus*. This subzone is 1.7 m thick in the Esna Formation (Table; Figure 2) and was dated as Ypresian. The *Blackites herculesii* Subzone (NP10b) is equivalent to Subzone NP10d of Aubry (1996) and Subzone NP10c of Tantawy (1998). The stratigraphic overlaps of *Tribrachiatus bramlettei* - *T. contortus* on one side and *T. contortus* - *T. orthostylus* on the other side are good guides to the completeness of Zone NP10 (Aubry, 1996; Dupuis et al., 2003; Raffi et al., 2005; Agnini et al., 2006; Tantawy, 2006; Abu Shama et al., 2007; Agnini et al. 2007a, 2007b). In the present study, short stratigraphic overlaps are documented between *T. bramlettei* and *T. contortus*, and between *T. contortus* and *T. orthostylus* (Table and Figure 2).

4.4. *Discoaster binodosus* Zone (NP11) (Mohler and Hay, in Hay and Mohler, 1967)

This zone ranges from the HO of *Tribrachiatus contortus* to the LO of *Discoaster lodoensis*. It is assigned to the Ypresian. This zone is 5 m thick and extends from the Esna Formation to the Thebes Formation, indicating a conformity between them (Table; Figure 2). The *Discoaster binodosus* Zone is correlative to Martini's (1971) Zone NP11 and Okada and Bukry's (1980) Subzone CP9b. The LO of *Tribrachiatus orthostylus* usually occurs shortly below the top of Zone NP10 and can approximately delineate Zone NP11 in case of the absence of *T. contortus*. Furthermore, the LO of *Sphenolithus radians* and the LO of *T. orthostylus* are coincident (Raffi et al., 2005; Agnini et al., 2007a) and can therefore approximately delineate the base of Zone NP11 when *T. contortus* is absent (Perch-Nielsen, 1985). The LOs of *S. radians* and *T. contortus* are coincident at the Misheiti Section (Table).

4.5. *Tribrachiatus orthostylus* Zone (NP12) (Brönnimann and Stradner, 1960)

This zone extends from the LO of *Discoaster lodoensis* to the HO of *Tribrachiatus orthostylus*. It was dated as Ypresian in age. About 0.8 m of this zone in the lowermost Thebes Formation was investigated in this study (Table; Figure 2). This zone is correlative to Zone CP10 of Okada and Bukry (1980) and Zone CNE4 of Agnini et al. (2014). Abu Shama et al. (2007) suggest placing the base of Zone NP12 between the LO of *Sphenolithus conspicuous* and the LO of *Neococcolithus dubius* in the case of poor preservation of *Discoaster lodoensis*. In the study section, the lower limit of the *T. orthostylus* Zone (NP12) was delineated by the LO of *D. lodoensis*.

5. Discussion

5.1. Calcareous nannofossil bioevents

Calcareous nannofossils are marked by significant changes before, during, and after the P/E boundary (e.g., Bukry, 1973; Romein, 1979; Aubry, 1996; Dupuis et al., 2003; Raffi et al., 2005; Tantawy, 2006; Agnini et al., 2007a, 2007b). These changes can be used for delineation of the P/E boundary and regional correlations when the marker beds, $\delta^{13}C$ and $\delta^{18}O$ excursions, and marker species are absent (Tantawy, 2006).

In Egypt, several authors documented calcareous nannofossil changes across the P/E boundary (see Aubry and Salem, 2013b and references therein; Faris et al., 2015; Al Wosabi, 2015). Biostratigraphic significances of calcareous nannofossil bioevents that were recorded in and/or close to the P/E boundary are summarized and discussed below.

5.1.1. The LO of *Discoaster multiradiatus*

Discoaster multiradiatus appeared about 1 million years before the P/E boundary (Agnini et al., 2014) and was considered a reliable marker for delineation of the base of Zone NP9 (Hay and Mohler, 1967; Okada and Bukry, 1980; Varol, 1989; Agnini et al., 2014; the present study, Table).

5.1.2. The LO and HO of the *Fasciculithus alanii* group

The last radiative episode of *Fasciculithus* occurs in the upper Paleocene (Romein, 1979). In the present study, several *Fasciculithus* species have their LOs in this interval; among them are *F. alanii*, *F. inversus*, *F. richardi*, *F. thomasii*, and *F. lillianiae* (Table). The LO of *F. alanii* always occurs in Subzone NP9a (Dupuis et al., 2003; Agnini et al., 2007b). Furthermore, the HO of *F. alanii* is close to the CIE (Dupuis et al., 2003). It was recorded in coincidence with the top of Subzone NP9a (Aubry and Salem; 2013a; Al Wosabi, 2015; Faris and Farouk, 2015). Therefore, it can be used to distinguish the pre-CIE part of Zone NP9 from the post-CIE part (Aubry and Salem, 2013a). However, Faris and Abu Shama (2007) had recorded *F. alanii* slightly above the NP9a/NP9b subzonal boundary. Moreover, Dupuis et al. (2003) suggested that specimens of *F. alanii* in the Dababiya Quarry Beds were reworked.

Agnini et al. (2007a) included fasciculith species with pentagon-like outlines (e.g., *Fasciculithus richardii*, *F. hayi*, *F. mitreus*, and *F. schaubii*) within the *Fasciculithus richardii* taxonomic group. Agnini et al. (2014) included all the fasciculith species that first appear in Zone NP9 into the *F. richardii* group, utilized the HO of this group to place the lower limit of the earliest Eocene Zone CNE1, and reported that this bioevent occurs before the LOs of *Rhomboaster* spp. In the present study, the fasciculith species that first appear in Zone NP9 are assigned to the *F. alanii* group, where the LO and HO of *F. alanii* are the most

significant bioevents in this group (Agnini et al., 2007a, 2007b; Aubry and Salem, 2013a). *Fasciculithus alanii* and *F. thomasii* disappear in the basal part of Subzone NP9b in the study section (Table).

5.1.3. The LOs and HOs of the Calcareous Nannofossil Excursion Taxa (CNET)

Calcareous Nannofossil Excursion Taxa are short-lived taxa, which appear suddenly and dominate the assemblages shortly after the onset of the PETM (Dupuis et al., 2003; Bown and Pearson, 2009). These taxa include *Discoaster araneus*, *D. anartios*, and *Rhomboaster* spp. and are therefore known as the *Rhomboaster-Discoaster* assemblage (RD; Kahn and Aubry, 2004). Other species such as *Bomolithus supremus*, *Coccolithus bownii*, *D. falcatus*, and *Toweius serotinus* were included in the CNET by Kahn and Aubry (2004).

The LOs of RD were utilized to subdivide Zone NP9 into two subzones (Aubry and Sanfilippo, 1999; Dupuis et al., 2003; Agnini et al., 2007a, 2007b; Faris and Farouk, 2015). However, the Eocene sequence at the GSSP starts at the base with an interval marked by carbonate dissolution (Dupuis et al., 2003) that prevents precise determination of the changes of nannofossil taxa across the P/E boundary (Raffi et al., 2005). In the study section, Zone NP9 is subdivided into Paleocene Subzone NP9a and Eocene Subzone NP9b based on the simultaneous LOs of *Rhomboaster* spp. (*R. cuspis*, *R. bitrifidia*, *R. spinosa*, and *R. intermedia*), *D. anartios*, and/or *D. araneus* (Table). No lithological change throughout this boundary was recorded in the study section (Figure 2).

5.1.4. The LO of *Discoaster mahmoudii*

Several authors documented the appearance of *Discoaster mahmoudii* within the upper portion of Zone NP9 (Dupuis et al., 2003; Agnini et al., 2007a; Aubry and Salem, 2013b). At Dababiya, *D. mahmoudii* appears about 3.5 m above the base of Eocene (Dupuis et al., 2003). Monechi et al. (2000) recorded *D. mahmoudii* at Wadi Nukhul (Egypt) directly above the CIE, and at about 2 m above the CIE at Gabal Oweina. They also recorded *D. mahmoudii* at about 7 m above the CIE at Gabal Nezzi, within the basal part of Zone NP10.

Aubry and Salem (2013b) proposed using the LOs of *D. mahmoudii*, *Pontosphaera minuta*, *Blackites solus* (*B. herculesii* herein), and/or the HO of *Fasciculithus alanii* to trace the base of Subzone NP9c when the RD assemblage is absent. In the present study, *D. mahmoudii* occurs just in one sample within Subzone NP9b (Table).

5.1.5. The LO of *Campylosphaera dela*

Bramlette and Sullivan (1961) originally described *Campylosphaera dela*, which was emended by Hay and Mohler (1967). Smaller and more elongate forms of *Campylosphaera* with narrow central areas that evolved in the early Eocene were described as *C. eodela* (Bukry and Percival 1971). However, the distinction between these two species is difficult, and they are here considered synonyms (Byble and Self-Trail, 1994).

Campylosphaera dela was used to subdivide the interval correlative to the *Discoaster multiradiatus* Zone (Bukry, 1973). However, inconsistent stratigraphic ranges for this taxon were documented by some authors (Agnini et al., 2007a). In the present study, *C. dela* is recorded earlier within Zone NP7/8 (Table). Due to the taxonomic disputes and different stratigraphic ranges, *C. dela* is considered an unreliable marker for biostratigraphic zonation.

5.1.6. The LO of *Discoaster binodosus*

Discoaster binodosus appears in the uppermost part of Zone NP9 (Perch-Nielsen, 1985). However, it was recorded near the base of Subzone NP9b (Faris and Salem, 2007) and within Zone NP10 (Faris and Farouk, 2015). In the study section, *D. binodosus* was recorded shortly above the base of Zone NP10 (Table). The LO of *D. binodosus*, therefore, seems to be a diachronous biohorizon as suggested by Faris and Salem (2007).

5.1.7. The decline of abundance and diversity of genus *Fasciculithus*

Previous studies revealed that the diversity of *Fasciculithus* species sharply declines near the top of the Paleocene (e.g., Raffi et al., 2005; Tantawy, 2006; Agnini et al., 2007a, 2007b). A similar finding is recorded in the study section, where the diversity of *Fasciculithus* decreases from 9 species in Subzone NP9a to 4 species at the top of Subzone NP9b, and disappears within Zone NP10 (Table). Furthermore, the relative abundance of *Fasciculithus* progressively decreases from 32% of the total assemblage in Subzone NP9a to 5%–9% in Subzone NP9b (Table).

5.1.8. The LOs and HOs of *Tribrachiatus* species

The LOs and HOs of *Tribrachiatus bramlettei*, *T. contortus*, *T. digitalis*, and *T. orthostylus* are biostratigraphically significant (Martini, 1971; Aubry, 1996). High-resolution studies reveal the occurrence of specimens of *T. bramlettei* shortly above the LO of *Rhomboaster* and the CIE (Agnini et al., 2007a, 2007b). However, the occurrence of *T. bramlettei* is discontinuous and rare to very rare in the early occurrences (Agnini et al., 2007b). Therefore, Faris et al. (2015) recommended using the common occurrence of *T. bramlettei* to place the base of Zone NP10. Moreover, calibrations of the earliest occurrence of *T. bramlettei* show large inconsistencies (Agnini et al., 2007a and references therein). These differences might be due to diachronism, or etching that usually occurs in the earliest Eocene sediments (Agnini et al., 2007a). Furthermore, some authors considered *T. bramlettei* and *R. cuspis* as synonyms (e.g., Von Salis et al., 2000). According this view, the bases of Zone NP10 and Subzone NP9b are coincident. Von Salis

et al. (2000) distinguished two subspecies of *R. bramlettei*: one with rays, *R. bramlettei bramlettei*, and another with corners, *R. bramlettei cuspis*. On the other hand, other authors believe that the structures of *T. bramlettei* and *Rhomboaster* species are different (e.g., Wei and Zhong, 1996; Raffi et al., 2005; Agnini et al., 2007a, 2007b). The later concept is followed in our study and *T. bramlettei* first occurs 0.6 m above the LO of *Rhomboaster* spp. (Table).

Several studies revealed that the HO of *Tribrachiatus bramlettei* occurs within the uppermost portion of Zone NP10, slightly after the disappearance of *T. contortus* and before the appearance of *T. orthostylus* (e.g., Aubry and Sanfilippo, 1999). However, Marzouk and Scheibner (2003) noted that *T. bramlettei* extends continuously up to the top of Zone NP10. In this study, *T. bramlettei* disappears directly below the LO of *T. orthostylus* (Table).

The *Tribrachiatus digitalis* morphotype and its range were subjected to criticism (Raffi et al., 2005) and it is therefore considered an unreliable marker. The LO of *T. orthostylus* can approximately delineate the top of Zone NP10 in the case of the absence of *T. contortus* (Perch-Nielsen, 1985). Two morphotypes of *T. orthostylus* are recognized at the top of Zone NP10: one form has three arms with slight bifurcations (Type A), and the other form is without bifurcations (Type B), which is common in the study section.

5.1.9. The HO of the genus *Fasciculithus*

The fasciculiths disappear in the lowermost Eocene (Martini, 1971; Backman, 1986; Raffi et al., 2005; Agnini et al., 2006; Tantawy, 2006; Agnini et al., 2007a, 2007b). Therefore, it was suggested to approximate the top of Zone NP9 by the HO of *Fasciculithus* when *Tribrachiatus bramlettei* is absent or very rare (Perch-Nielsen, 1985; Tantawy, 2006). However, several *Fasciculithus* species (*F. involutus*, *F. tympaniformis*, *F. liliiani*, *F. alanii*, *F. schaubii*, and/or *F. thomasii*) were recorded within Zone NP10 (Romein, 1979; Aubry, 1996; Tantawy 1998; Raffi et al., 2005; Tantawy, 2006; Agnini, 2007a). This makes it difficult to know whether they are survived, they are reworked, or their occurrences are diachronous. This is probably due to the taxonomic disputes concerning the position of *T. bramlettei* in the *Rhomboaster-Tribrachiatus* lineage (Tantawy, 2006). Agnini et al. (2014) used the HO of *F. tympaniformis* to delineate the top of the earliest Eocene Zone CNE1. In the present study, most fasciculiths disappear in Zone NP9; however, *F. tympaniformis*, *F. involutus*, and *F. thomasii* extended to Zone NP10. In addition, *F. tympaniformis* is common up to the upper portion of Zone NP10 (Table).

5.1.10. The LO of *Discoaster diastypus*

The LOs of *Tribrachiatus contortus* and *Discoaster diastypus* were considered synchronous (Bukry, 1973; Raffi et al., 2005). Bukry (1973) used these two bioevents to delineate the base of *Discoaster diastypus* Zone that is Okada and Bukry's (1980) Zone CP9. *Discoaster diastypus* occurs with *T. bramlettei* in several Egyptian sections (Tantawy, 2006; Abu Shama et al., 2007). However, Tantawy (2006) recorded *D. diastypus* about 1.5 m below the LO of *T. bramlettei* at Taramsa, South Egypt. On the other hand, Faris and Salem (2007) recorded the LO of *D. diastypus* about 1 m above the LO of *T. bramlettei*. In the study section, *D. diastypus* was recorded shortly above the first occurrence of *T. bramlettei* (Table). These inconsistencies confirm the diachronism of *T. bramlettei* and/or *D. diastypus*.

5.1.11. The LO of *Sphenolithus radians*

The HO of *Tribrachiatus contortus* and the LO of *Sphenolithus radians* are closely related (Perch-Nielsen, 1985). Therefore, the LO of *S. radians* can delineate the top of Zone NP10 in the case of the absence of *T. contortus* (Perch-Nielsen, 1985). Abu Shama et al. (2007) and Al Wosabi (2015) recorded *S. radians* up to the uppermost of Zone NP11 and suggested using it to mark the top of Zone NP11. In our present study, the earliest appearance of *S. radians* occurs within Subzone NP10b in coincidence with the LO of *T. contortus* (Table).

5.1.12. The HO of *Discoaster multiradiatus*

The occurrence of *Discoaster multiradiatus* is supposed to extend to the basal portion of Zone NP11 (Perch-Nielsen, 1985). However, *D. multiradiatus* disappears within Subzone NP10b at the Misheiti Section (Table).

5.1.13. The acme of *Ericsonia subpertusa*

At the GSSP for the base of the Eocene, an acme of *Ericsonia subpertusa* was documented in coincidence with the CIE (Dupuis et al., 2003). Similar findings were recorded in several sections (Abu Shama et al., 2007). In the present study, *Coccolithus pelagicus* and *E. subpertusa* are most dominant around the P/E boundary (Table).

5.1.14. The LO of *Blackites herculesii*

Rhabdosphaera herculea was introduced by Stradner (1969) and later assigned to *Rhabdolithus solus* by Perch-Nielsen (1971) and named *Blackites herculesii* by Bybell and Self-Trail (1997). It was recorded within the uppermost of Zone NP9 (Faris and Salem, 2007; Aubry and Salem, 2013a). The LO of *B. solus* can be used to distinguish between Subzones NP9a and NP9c in the case of the absence of the RD assemblage (Aubry and Salem, 2013a). It occurs in the base of Zone NP10 at the Misheiti Section (Table).

5.2. The calcareous nannofossil species richness and abundance

The number of calcareous nannofossil species reaches a first maximum in the Paleogene within Zone NP9 (Perch-Nielsen, 1985). In the present study, most *Discoaster* species that mark the Paleocene first appear near the top of the Paleocene (Table). *Fasciculithus* and *Rhomboaster* evolve and diversify within Zone NP9 (Table). The species

richness of calcareous nannofossils reaches 24 species and 28 species within the upper portion of Zone NP9 and the basal part of Zone NP10, respectively. In addition, the abundance of calcareous nannofossils reaches its maximum (12 S/FOV) within Subzone NP9b (Table).

5.3. Stable isotopes

The $\delta^{13}C$ and $\delta^{18}O$ isotopic records are dependent on water temperature and the isotope composition of sea water (Stassen et al., 2009). Therefore, they provide a valuable indicator and widely used tool for tracking the water paleotemperatures and variations in biogenic and oceanographic conditions. Globally, the P/E boundary was associated with abrupt negative $\delta^{13}C$ and $\delta^{18}O$ excursions (Dupuis et al., 2003). At the Misheiti section, the carbonate content as well as the $\delta^{13}C$ and $\delta^{18}O$ were measured in selected bulk-rock samples as shown in Figure 3. In the study section, the $\delta^{13}C$ decreases from 1.41‰ to –0.58‰ across the NP9a/NP9b subzonal boundary, and the $\delta^{18}O$ decreases from –2.88‰ to –4.83‰.

5.4. Carbonate content

The base of the Eocene in Egypt was often delineated at the base of an interval of carbonate dissolution (Aubry et al., 1996; Raffi et al., 2005; Zachos et al., 2005; Agnini et al., 2007a, 2007b). A similar carbonate dissolution event was documented in the Dababiya GSSP section as well as several Egyptian sections (Dupuis et al., 2003; Tantawy, 2006; Khozyem et al., 2013). Tantawy (2006) recorded *Campylosphaera* (*eo*)*dela*, *Discoaster araneus*, and *Fasciculithus richardii* at about 5 cm below the dissolution interval, whereas *Rhomboaster* spp. occur just above this interval at the Gabal Serai section, Nile Valley, Egypt. However, he recorded all these taxa slightly above the dissolution interval at the Taramsa section, Nile Valley, Egypt. In the present study, the calcium carbonate content drops sharply to 32.3% below the P/E boundary and increases slightly to 45.62% above it (Figure 3).

5.5. Remarks

The Paleocene-Eocene interval is characterized by lithologic, geochemical, and paleontological changes (El Deeb et al., 2000; Dupuis et al., 2003; Agnini et al., 2007a, 2007b; Aubry et al., 2007). The P/E boundary was delineated either within calcareous nannofossil Zone NP9, in Zone NP10, or coincident with the lower limit of Zone NP10 (Martini, 1971; Perch-Nielsen, 1985). Bukry (1973) delineated this boundary by the LO of *Discoaster diastypus*, which is somewhat higher in Zone NP10 (Romein, 1979). In Egypt, it was traditionally placed at the base of Zone NP10 or within Zone NP10 (Bolle et al., 2000). The LOs of *Discoaster diastypus*, *T. bramlettei*, and *D. binodosus* were used by Faris (1993) to trace the base of the Eocene. Later, the base of the Eocene was placed at the GSSP in coincidence with the base of calcareous nannofossil Subzone NP9b (Dupuis et al., 2003). At several Egyptian sections, the P/E boundary was delineated at the base of Subzone NP9b (e.g., Tantawy, 2006; Faris and Salem, 2007; Faris and Farouk, 2015). In this study, the P/E boundary is placed at the base of Subzone NP9b that is delineated by the LOs of *Rhomboaster* spp., *Discoaster anartios*, and/or *D. araneus* (Table). It cuts across the lowermost Esna Formation without remarkable lithological changes (Figure 2).

6. Summary

Calcareous nannofossil, $\delta^{13}C$, $\delta^{18}O$, and carbonate content variations across the P/E interval were revealed at the Misheiti Section. The uppermost Tarawan, Esna, and lowermost Thebes formations were included in the present study. Lithologically, the Esna Formation was informally differentiated into the Hanadi/Mahmiya and Abu Had members. Four calcareous nannofossil zones (NP9, NP10, NP11, and NP12) are recognized. Zone NP9 of Martini (1971) is further divided into two subzones, the *Fasciculithus alanii* Subzone (NP9a) and the *D. araneus* Subzone (NP9b), on the basis of the LOs of *Rhomboaster* spp., *Discoaster araneous*, and/or *D. anartios*. Martini's (1971) Zone NP10 is also subdivided into two subzones, the *Tribrachiatus bramlettei* (NP10a) and the *Blackites herculesii* Subzones (NP10b), based on the LO of *Tribrachiatus contortus* that is coincident with the LO of *Sphenolithus radians*. *Discoaster diastypus* and *D. binodosus* are recorded slightly above the base of Zone NP10.

Fasciculith species that first appear in Zone NP9 are assigned to the *F. alanii* group in the present study. Most fasciculith species disappear in Subzone NP9a; however, *F. involutus*, *F. alanii*, and *F. thomasii* disappear within the lowermost part of Subzone NP9b, whereas *F. tympaniformis* extends with common occurrence to Subzone NP10b. *Blackites herculesii* first appears at the basal part of Zone NP10, whereas *Zygrhablithus bijugatus* unusually appears above the extinction of *Fasciculithus* spp. Blooms of *Ericsonia subpertusa* and *Coccolithus pelagicus* as well as an increase of calcareous nannofossil diversity and abundance were recorded across the P/E boundary interval. The base of the Eocene is coincident with the base of Subzone NP9b and cuts across the basal part of the Esna Formation without any distinctive lithological change. The global drops of $\delta^{13}C$, $\delta^{18}O$, and calcium carbonate content marking the P/E boundary were recorded in the study section.

Acknowledgments

We are grateful to Professor Michael Wagreich and Professor Ercan Özcan for their careful reviews, constructive comments, and helpful suggestions that improved the manuscript.

References

Abdel Razik TM (1972). Comparative studies on the Upper Cretaceous–Early Paleogene sediments on the Red Sea coast, Nile Valley and Western Desert, Egypt. In: 6th Arab Petroleum Congress, Algeria, pp. 1-23.

Abu Shama A, Faris M, Al-Wosabi K (2007). Upper Paleocene–lower Eocene calcareous nannofossil biostratigraphy and paleoecology of Gebel Matulla section, Southwestern Sinai, Egypt. In: Proceedings of the 5th International Conference on the Geology of Africa, Assiut, Egypt, pp. 33-51.

Agnini C, Fornaciari E, Raffi I, Catanzariti R, Pälike H et al. (2014). Biozonation and biochronology of Paleogene calcareous nannofossils from low and middle latitudes. Newsletters on Stratigraphy, Stuttgart 47/2: 131-181. doi: 10.1127/0078-0421/2014/0042

Agnini C, Fornaciari E, Raffi I, Rio D, Röhl U et al. (2007a). High-resolution nannofossil biochronology of middle Paleocene to early Eocene at ODP Site 1262: implications for calcareous nannoplankton evolution. Marine Micropaleontology 64: 215-248. doi: 10.1016/j.marmicro.2007.05.003

Agnini C, Fornaciari E, Rio D, Tateo F, Backman J et al. (2007b). Responses of calcareous nannofossil assemblages, mineralogy and geochemistry to the environmental perturbations across the Paleocene/Eocene boundary in the Venetian Pre-Alps. Marine Micropaleontology 63: 19-38. doi: 10.1016/j.marmicro.2006.10.002

Agnini C, Muttoni G, Kent DV, Rio D (2006). Eocene biostratigraphy and magnetic stratigraphy from Possagno, Italy: the calcareous nannofossil response to climate variability. Earth and Planetary Science Letters 241: 815-830. doi: 10.1016/j.epsl.2005.11.005

Al Wosabi KA (2015). Calcareous nannofossils biostratigraphy and paleoecology of the Late Paleocene/Early Eocene of Wadi Nukhul West Central Sinai, Egypt. Earth Sciences 4/2: 59-71. doi: 10.11648/j.earth.20150402.11

Aubry MP (1996). Towards an upper Paleocene–lower Eocene high resolution stratigraphy based on calcareous nannofossil stratigraphy. Israel Journal of Earth Science 44: 239-253.

Aubry MP, Berggren WA, Cramer B, Dupuis C, Kent DV et al. (1999). Paleocene/Eocene boundary sections in Egypt. In: Late Paleocene–Early Eocene Events from Northern Africa to the Middle East. International Symposium in Connection with 1st International Conference on the Geology of Africa, Assiut, Egypt, pp. 1-11.

Aubry MP, Ouda K, Dupuis C, Berggren WA, Van Couvering JA et al. (2007). The Global Standard Stratotype-Section and Point (GSSP) for the base of the Eocene Series in the Dababiya section (Egypt). Episodes 30 (4): 271-286. doi: 10.18814/epiiugs/2007/v30i4/003

Aubry MP, Salem R (2013a). The Dababiya Quarry Core: Coccolith biostratigraphy. Stratigraphy 9: 241-259.

Aubry MP, Salem R (2013b). The Dababiya Core: a window into Paleocene to Early Eocene depositional history in Egypt based on coccolith stratigraphy. Stratigraphy 9: 287-346.

Aubry MP, Sanfilippo A (1999). Late Paleocene–Early Eocene sedimentary history in western Cuba: implications for the LPTM and for regional tectonic history. Micropaleontology 45: 5-18. doi: 10.2307/1486101

Awad GH, Ghobrial MG (1965). Zonal Stratigraphy of the Kharga Oasis. Ministry of Industry, General Egyptian Organization for Geological Research and Mining, Paper No. 34. Cairo, Egypt: Geological Survey.

Backman J (1986). Late Paleocene to middle Eocene calcareous nannofossil biochronology from the Shatsky Rise, Walvis Ridge and Italy. Paleogeography, Paleoclimatology and Paleoecology 57: 43-59. doi: 10.1016/0031-0182(86)90005-2

Bains S, Corfield RM, Norris RD (1999). Mechanisms of climate warming at the end of the Paleocene. Science 285: 724-727. doi: 10.1126/science.285.5428.724

Beadnell HJL (1905). The relation of the Eocene and Cretaceous systems in the Esna-Aswan Reach of the Nile Valley. Journal of the Geological Society (London) 61: 667-676. doi: 10.1144/GSL.JGS.1905.061.01-04.35

Berggren WA, Aubry MP (1996). A late Paleocene-early Eocene NW European and North Sea magnetochronologic correlation network. In: Knox RWOB, Corfield RM, Dunay RE (editors). Correlation of the Early Paleogene in Northwestern Europe. London, UK: Geological Society of London Special Publications, pp. 309-352.

Bolle MP, Tantawy A, Pardo A, Adatte T, Burns S et al. (2000). Climate and environmental changes documented in the upper Paleocene to lower Eocene of Egypt. Eclogae Geologicae Helvetiae 93: 33-51.

Bown PR, Pearson P (2009). Calcareous plankton evolution and the Paleocene/Eocene thermal maximum event: new evidence from Tanzania. Marine Micropaleontology 71: 60-70. doi: 10.1016/j.marmicro.2009.01.005

Bown PR, Young JR (1998). Techniques. In: Bown PR (editor). Calcareous Nannofossil Biostratigraphy. British Micropalaeontological Society Publication Series. London, UK: Chapman & Hall, pp. 16-28.

Bramlette MN, Sullivan FR (1961). Coccolithophorids and related nannoplankton of the Early Tertiary in California. Micropaleontology 7: 129-188.

Brönnimann P, Stradner H (1960). Die foraminiferen und Discoasteridenzonen von Kuba und ihre intercontinental correlation. Erdoel 76: 364-369 (in German).

Bukry D (1973). Low latitude coccoliths biostratigraphic zonation. In: Initial Reports of the Deep Sea Drilling Project, 15. Washington, DC, USA: US Government Printing Office, pp. 685-703.

Bukry D, Percival SF (1971). New Tertiary calcareous nannofossils. Tulane Studies in Geology and Paleontology 8 (3): 123-146.

Bybell LM, Self-Trail JM (1997). Late Paleocene and early Eocene calcareous nannofossils from three boreholes in an onshore–offshore transect from New Jersey to the Atlantic continental rise. In: Miller KG, Snyder SW (editors). Proceedings of Ocean Drilling Program Scientific Results, 150X (1997). College Station, TX, USA: Ocean Drilling Program, pp. 91-110. doi: 10.2973/odp.proc.sr.150x.307.1997

Dupuis C, Aubry MP, Steurbaut E, Berggren WA, Ouda K et al. (2003). The Dababiya quarry section: lithostratigraphy, clay mineralogy, geochemistry and paleontology. Micropaleontology 49: 41-59. doi: 10.2113/49.Suppl_1.41

El Deeb WZ, Faris M, Mandur M (2000). Upper Cretaceous-Lower Paleogene foraminiferal paleoecology of north and southwest Sinai areas, Egypt. Egyptian Journal of Petroleum 9: 105-122.

Faris M (1993). Calcareous nannofossil events at the Paleocene-Eocene boundary in Egypt. Bulletin of Faculty of Science, Qena, Assiut University, Egypt 1/2: 89-99.

Faris M, Abu Shama A (2007). Nannofossil biostratigraphy of Paleocene-lower Eocene succession in the Thamad area, east central Sinai, Egypt. Micropaleontology 53 (1): 127-144. doi: 10.2113/gsmicropal.53.1-2.127

Faris M, Farouk S (2015). Calcareous nannofossils of the Paleocene-Eocene transition in four sections from Egypt. Turkish Journal of Earth Sciences 24: 585-606. doi:10.3906/yer-1411-25

Faris M, Ghandour IM, Zahran E, Mosa G (2015). Calcareous nannoplankton changes during the Paleocene-Eocene Thermal Maximum in West Central Sinai, Egypt. Turkish Journal of Earth Sciences 24 (5): 475-493. doi: 10.3906/yer-1412-34

Faris M, Salem R (2007). Paleocene-Eocene calcareous nannofossil biostratigraphy in west central Sinai, Egypt. In: Proceedings of the 8th Conference of Geology of Sinai for Development Ismailia, Egypt, pp. 1-14.

Gardin S, Monechi S (1998). Palaeoecological change in middle to low latitude calcareous nannoplankton at the Cretaceous/Tertiary boundary. Bulletin de la Société Géologique de France 169 (5): 709-723.

Hay WW (1964). The use of the electron microscope in the Study of Fossils. Smithsonian Institution Annual Reports 1963: 409-415.

Hay WW, Mohler HP (1967). Calcareous nannoplankton from early Tertiary rocks at Pont Labau, France, and Paleocene–early Eocene correlations. Journal of Paleontology 41 (6): 1505-1541.

Jiang MJ, Gartner S (1986). Calcareous nannofossil succession across the Cretaceous–Tertiary boundary in east-central Texas. Micropaleontology 32: 232-255. doi: 10.2307/1485619

Kahn A, Aubry MP (2004). Provincialism associated with the Paleocene/Eocene Thermal Maximum: temporal constraint. Marine Micropaleontology 52: 117-132. doi: 10.1016/j.marmicro.2004.04.003

Kasem AM, Wise S Jr., Faris M, Farouk S, Zahran E (2017a). Calcareous nannofossil biostratigraphy of the uppermost Maastrichtian–lower Paleocene at the Misheiti section, East Central Sinai, Egypt. Revue de Micropaleontology 60: 179-192. doi: 10.1016/j.revmic.2017.05.002

Kasem AM, Wise S Jr., Faris M, Farouk S, Zahran E (2017b). Calcareous nannofossil biostratigraphy of the Paleocene at the Misheiti section, East Central Sinai, Egypt. Arabian Journal of Geosciences 10: 455. doi: 10.1007/s12517-017-3217-4

Khozyem H, Adatte T, Spangenberg JE, Tantawy A, Keller G (2013). Paleoenvironmental and climatic changes during the Paleocene-Eocene Thermal Maximum (PETM) at the Wadi Nukhul Section, Sinai, Egypt. Journal of the Geological Society of London 170: 341-352. doi: 10.1144/jgs2012-046

Martini E (1971). Standard Tertiary and Quaternary calcareous nannoplankton zonation. In: Farinacci A (editor). Proceedings of the 2nd Planktonic Conference, Rome, Italy (1970), pp. 739-785.

Marzouk AM, Scheibner C (2003). Calcareous nannoplankton biostratigraphy and paleoenvironment of the late Cretaceous-Paleogene of the Galala Mountains, Eastern Desert, Egypt. Courier Forschungsinsitut Senckenberg 244: 11-35.

Monechi S, Angori E, Speijer RP (2000). Upper Paleocene biostratigraphy in the Mediterranean region: Zonal markers, diachronism, and preservational problems. In: Andreasson FP, Schmitz B, Thompson EI (editors). Early Paleogene Warm Climates and Biosphere Dynamics, GFF, pp. 108-110. doi: 10.1080/11035890001221108

Okada H, Bukry D (1980). Supplementary modification and introduction of code numbers to the low-latitude coccolith biostratigraphic zonation (Bukry, 1973; 1975). Marine Micropaleontology 5: 321-325. doi: 10.1016/0377-8398(80)90016-X

Perch-Nielsen K (1971). Elektronenmikroskopische untersuchungen an Coccolithen und verwandten Formen aus dem Eozan von Danemark. Biologiske Skrifter. Kongelige Danske Videnskabernes Selskab 18 (3): 1-76 (in German).

Perch-Nielsen K (1985). Mesozoic calcareous nannofossils. In: Bolli HM, Saunders JB, Perch-Nielsen K (editors). Plankton Stratigraphy. Cambridge, UK: Cambridge University Press, pp. 329-426.

Raffi I, Backman J, Pälike H (2005). Changes in calcareous nannofossil assemblage across the Paleocene/Eocene transition from the paleo-equatorial Pacific Ocean. Palaeogeography, Palaeoclimatology, Palaeoecology 226: 93-126. doi: 10.1016/j.palaeo.2005.05.006

Robert C, Kennett JP (1992). Paleocene and Eocene kaolinite distribution in the South Atlantic and Southern Ocean: Antarctic climatic and paleoceanographic implications. Marine Geology 103: 99-110. doi: 10.1016/0025-3227(92)90010-F

Romein AJT (1979). Lineages in Early Paleocene nannoplankton. Utrecht Micropaleontology Bulletin 22: 18-22.

Said R (1960). Planktonic foraminifera from the Thebes Formation, Luxor, Egypt. Micropaleontology 6: 277-286. doi: 10.2307/1484234

Sluijs A, Schouten S, Pagani M, Woltering M, Brinkhuis H et al. (2006). Expedition 302 Scientists Subtropical Arctic Ocean temperatures during the Palaeocene/Eocene thermal maximum. Nature 441: 610-613. doi: 10.1038/nature04668

Stassen P, Dupuis C, Morsi AM, Steurbaut E, Speijer RP (2009). Reconstruction of a latest Paleocene shallow-marine eutrophic paleoenvironment at Sidi Nasseur (Central Tunisia) based on foraminifera, Ostracoda, calcareous nannofossils and stable isotopes (δ13C, δ18O). Geologica Acta 7: 93-112. doi: 10.1344/105.000000273

Stradner H (1969). The nannofossils of the Eocene Flysch in the Hagenbach Valley (Northern Vienna Woods) Austria. Rocznik Polskiego Towarzystwa Geologicznego 39: 403-432.

Tantawy A (2006). Calcareous nannofossil of the Paleocene–Eocene transition at Qena Region, Central Nile Valley, Egypt. Micropaleontology 52 (3): 193-222. doi: 10.2113/gsmicropal.52.3.193

Thomas E, Zachos JC, Bralower TJ (2000). Ice-free to glacial world transition as recorded by benthic foraminifera. In: Huber BT, MacLeod KG, Wing SL (editors). Warm Climates in Earth History. Cambridge, UK: Cambridge University Press, pp. 132-160.

Tremolada F, Bralower TJ (2004). Nannofossil assemblage fluctuations during the Paleocene–Eocene Thermal Maximum at Sites 213 (Indian Ocean) and 401 (North Atlantic Ocean): palaeoceanographic implications. Marine Micropaleontology 52: 107-116. doi: 10.1016/j.marmicro.2004.04.002

Varol O (1989). Palaeocene calcareous nannofossil biostratigraphy. In: Crux JA, Van Heck SE (editors). Nannofossils and Their Applications. London, UK: British Micropaleontological Society, pp. 267-310.

Von Salis K, Monechi S, Bybell LM, Self-Trail J, Young JR (2000). Remarks on the calcareous nannofossil genera *Rhomboaster* and *Tribrachiatus* around the Paleocene/Eocene Boundary. In: Andreasson FP, Schmitz B, Thompson EI (editors). Early Paleogene Warm Climates and Biosphere Dynamics, GFF, pp. 138-140. doi: 10.1080/11035890001221138

Wei W, Zhong S (1996). Taxonomy and magnetobiochronology of *Tribrachiatus bramlettei* and *Rhomboaster*: two genera of calcareous nannofossils. Journal of Paleontology 70 (1): 7-22. doi: 10.1017/s0022336000023064

Westerhold T, Röhl U, McCarren HK, Zachos JC (2009). Latest on the absolute age of the Paleocene–Eocene Thermal Maximum (PETM): new insights from exact stratigraphic position of key ash layers + 19 and – 17. Earth and Planetary Science Letters 287: 412-419. doi: 10.1016/j.epsl.2009.08.027